Pressure-induced structural phase transition in the ferromagnetic Heusler alloy Ni_2MnGa

T. Eto,[1,*] Y. Nakamoto,[2] T. Kagayama,[2] Y. Adachi,[3] S. Kawaguchi,[4] N. Hirao,[4] Y. Uwatoko,[5] M. Nagasako,[6] and T. Kanomata[7]

[1]*Kurume Institute of Technology, Kurume 830-0052, Japan*
[2]*KYOKUGEN, Graduate School of Engineering Science, Osaka University, Toyonaka 560-8531, Japan*
[3]*Graduate School of Science and Engineering, Yamagata University, Yonezawa 992-8510, Japan*
[4]*JASRI/SPring-8, Kouto, Sayo-cho, Sayo-gun, Hyogo 679-5198, Japan*
[5]*Institute for Solid State Physics, The University of Tokyo, Kashiwa 277-8581, Japan*
[6]*Institute for Materials Research, Tohoku University, Sendai 980-8577, Japan*
[7]*Research Institute for Engineering and Technology, Tohoku Gakuin University, Sendai 984-8588, Japan*

(Received 3 November 2022; revised 1 December 2023; accepted 4 December 2023; published 3 January 2024)

The effect of pressure on the crystal structure of Ni_2MnGa was investigated up to 41 GPa using *in situ* angle-dispersive x-ray diffraction with synchrotron radiation, an imaging plate detector, and a diamond anvil cell. A pressure-induced transition from a cubic $L2_1$ structure (space group $Fm\bar{3}\,m$) to a 10-layer modulated monoclinic structure ($C2/m$) with a distortion of $\beta \sim 92^\circ$ occurred at a pressure of 19.1 GPa or lower. The volume change at the martensitic transition is a minute value of about -0.1%. The bulk modulus for the low-pressure phase is 147(2) GPa, consistent with previous studies. In contrast, the bulk modulus for the high-pressure phase is 229(4) GPa, significantly higher than the former bulk modulus. Initial permeability measurements of the Ni_2MnGa were also conducted at various pressures up to 1 GPa. The pressure dependencies of the Curie temperature, premartensitic, and martensitic transition temperatures are discussed in detail.

DOI: 10.1103/PhysRevB.109.014101

I. INTRODUCTION

The Ni_2MnGa alloy has received a great deal of interest in recent years as a candidate for functional materials, exhibiting magnetic shape memory effects (MSMEs) [1], large magnetic field induced strain (MFIS) [2], and magnetocaloric effect (MCE) [3,4]. The alloy has a cubic $L2_1$ structure with a space group of $Fm\bar{3}\,m$, and exhibits a ferromagnetic transition at Curie temperature, $T_C \sim 376$ K, without any change in crystal structure [1]. Upon cooling below T_C, the ferromagnetic austenite (A) phase undergoes premartensitic (PM) and martensitic (M) transitions at $T_{PM} \sim 260$ K [5–7] and $T_M \sim 210$ K [1], respectively. In the PM phase, lattice softening occurs due to a decrease in the shear elastic constant [5,8–12], resulting in a 3M-like incommensurate structure [7]. Below the PM phase transition temperature, it has been reported that 10-layer modulated monoclinic (10M) and 14-layer modulated monoclinic (14M) structures appear continuously during the cooling process in stoichiometric Ni_2MnGa [13–15].

Varying the compositional ratio of the Ni-Mn-Ga compounds results in a variety of magnetic properties, transport properties, and crystal structures, leading to interesting phase diagrams [14–19]. For example, in alloys such as $Ni_{2+x}Mn_{1-x}Ga$, $Ni_2Mn_{1+y}Ga_{1-y}$, and $Ni_{2+x}MnGa_{1-x}$, the M phase undergoes a transition from the 10M or 14M modulated structures to a non-modulated tetragonal structure ($L1_0$ type) when the total electron number e/a exceeds ~7.6. In this e/a region, the first-order structural phase transition coincides with the magnetic transition, a phenomenon known as "magnetostructural coupling," and large magneto-caloric effects can be expected. Furthermore, in the region of $e/a > 7.7$, T_M increases rapidly in the paramagnetic martensite phase, presenting potential applications in the shape memory alloys at high temperatures. Therefore, for the application of Heusler alloys as functional materials, it is crucial to investigate the key factor for each phase transition phenomenon. Thus far, several studies on Heusler alloys have been conducted by varying element substitutions and their compositions, which were accompanied by what is known as "chemical pressure." However, this approach may have a drawback of introducing secondary effects such as lattice defects and impurity effects, making it challenging to detect minute changes in various physical properties. Pressure is effective in suppressing these secondary effects, resulting in simple lattice contraction.

We conducted hydrostatic pressure experiments on Ni_2MnGa to explore structural changes, such as the M and PM transitions [20–23], magnetic properties related to Curie temperature and magnetization [24,25], and thermal properties associated with MCE [26–28]. These experiments were performed in the low-pressure region, reaching a maximum of about 1 GPa; more work needs to be done to detail pressure-induced structural phase transitions in Ni_2MnGa in the high-pressure region. Furthermore, with the exception of ultrasonic experiments and first-principles calculations, there have been no investigations into the bulk moduli of the austenitic and martensitic phases of Ni-Mn-Ga alloys based on compression curves. This study aims to investigate effects

*teto@kurume-it.ac.jp

of lattice constants and interatomic distances on the crystal structure and magnetism under pressure, providing further insights into the physical properties of Ni_2MnGa within the framework of the *p-T* phase diagram.

II. EXPERIMENT

A polycrystalline sample of Ni_2MnGa was prepared by repeated arc melting of appropriate quantities of constitutionally pure elements, namely, 99.99% Ni, 99.9% Mn, and 99.9999% Ga, in an argon atmosphere. The ingot was turned upside down and remelted more than four times for each composition to obtain good compositional homogeneity. The resulting ingot was sealed in evacuated silica tubes, annealed at 850 °C for 3 days, and then quenched in cold water. The composition of the sample was confirmed using inductively coupled plasma mass spectrometry (ICPMS), revealing a nearly stoichiometric ratio of Ni: 1.98, Mn: 0.99, and Ga: 1.03. After pulverization, the sample underwent a 2-day heat treatment at 500 °C for x-ray powder diffraction (XRPD) and initial permeability measurement. The crystal structure was identified from XRPD data measured at room temperature (RT) and ambient pressure using Cu $K\alpha$ radiation, and Rietveld analysis was conducted using the RIETAN-FP software package [29].

We investigated the crystal structure of Ni_2MnGa under high pressure at RT using *in situ* angle-dispersive x-ray diffractometry at BL10XU in SPring-8, employing monochromatized synchrotron radiation and an imaging plate detector [30]. The x-ray beam monochromated to a wavelength of $\lambda = 0.413\,28$ Å ($E = 30$ keV) was focused by using a SU-8 polymer compound refractive lens. High pressure was generated with a diamond anvil cell (DAC). We used a diamond anvil with an inner culet of 300 μm. Powdered Ni_2MnGa was filled in a 100 μm diameter hole in a preindented rhenium gasket of 30–35 μm thickness, together with a helium (He) pressure medium compressed to 200 MPa by a high-pressure gas-loading system in SPring-8. He gas was chosen to maintain the sample under hydrostatic conditions. Additionally, a small amount of ruby powder was enclosed as a pressure marker in the gasket hole, and the pressures were determined using the ruby gauge of Zha *et al.* [31]. During the experiment, XRPD images were collected at three positions (A, B, and C) near the center of the DAC. We measured up to a maximum pressure of 41.2 GPa for positions A and B but limited measurements to 32.3 GPa at position C to optimize the measurement time at the synchrotron radiation facility.

The Curie temperature T_C both at ambient and high pressure was determined using an ac transformer method, in which primary and secondary coils were wound on the sample. An ac current of constant amplitude was applied to the primary coil and voltage across the secondary coil, which is directly proportional to initial permeability μ, was recorded as a function of temperature at various pressures. Hydrostatic pressure was applied using a Teflon pressure cell filled with Daphne oil and incorporating a piston-cylinder type mechanism. In this Teflon cell, the sample was placed in a cylindrical holder made of boron nitride with high thermal conductivity. A schematic diagram of the apparatus is provided in Ref. [32].

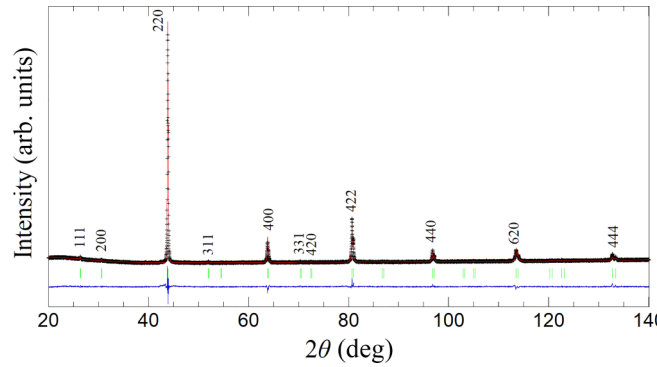

FIG. 1. (a) Rietveld refinement of the RT XRPD pattern for Ni_2MnGa at ambient pressure. The experimental data, fitted curve, and the residue are shown by the cross (black), continuous line (red), and bottom-most plot (blue), respectively. The tick marks (green) represent the Bragg peak positions. The final fit resulted in reliability factors of $R_{wp} = 3.22\%$, $R_p = 2.21\%$, and $R_B = 4.79\%$.

III. RESULTS AND DISCUSSION

A. Powder x-ray diffraction

Figure 1 shows a XRPD pattern of Ni_2MnGa at ambient pressure and RT. The observation that all diffraction lines can be indexed with the Heusler austenite $L2_1$ structure (space group: $Fm\bar{3}m$) and exhibit superlattice diffractions of 111 and 200 indicates that the sample is a single phase with well-ordered atomic positions. The lattice parameters a_c of the cubic cell are determined to be 5.822 06(10) Å through Rietveld analysis, aligning with the findings of Webster *et al.* [1].

Figure 2 shows typical XRPD patterns at position A for various pressures. In the figure, diffraction peaks are indexed as the cubic $L2_1$ structure up to 21.6 GPa. While all x-ray diffraction lines at 23.9 GPa initially appear to be indexed with the $L2_1$ structure, additional diffraction lines (indicated by arrows) emerge beside the 220 main peak, as shown in the inset. Above 27.5 GPa, the diffraction patterns suggest the stability of a high-pressure martensitic structure, distinct from the $L2_1$ austenitic structure.

The x-ray diffraction patterns near the transition pressure at position B are shown in Fig. 3. At 17.0 GPa, only the main 220 diffraction line is observed. However, at pressures of 19.1 and 19.7 GPa, two or three subpeaks emerge, resembling the pattern of 23.9 GPa at position A (see Fig. 2 inset). That is, the pressure-induced structural phase transition from the low-pressure austenite (LPA) phase to the high-pressure martensite (HPM) phase occurs at pressures of 19.1 GPa or lower. Thus, both scenarios, with and without the phase transition around 19 GPa, coexist within the same DAC. Helium is currently recognized as the most hydrostatic pressure medium [33]. Although helium solidifies above approximately 12 GPa at RT, it remains almost hydrostatic up to about 30 GPa and gradually becomes nonhydrostatic beyond that pressure. While the reason for the discrepancy in the structural phase transition pressure is not yet clear, a slight strain induced at sample position A may contribute to the difference. It seemed that the gasket hole of the DAC contracted with increasing pressure,

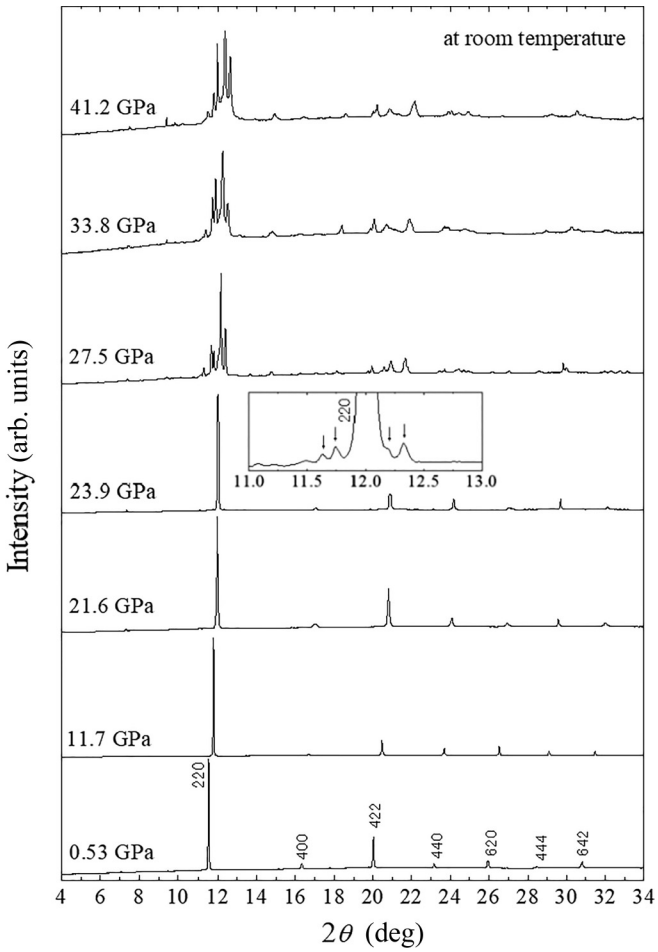

FIG. 2. The RT XRPD patterns of Ni_2MnGa at position A under various pressures. The inset provides an enlarged scale view of the pattern around the main peak at 23.9 GPa.

causing the edge of the rhenium gasket to impact near sample position A.

The RT XRPD pattern of Ni_2MnGa observed under a pressure of 30.2 GPa at position A is shown in Fig. 4(a) as a representative example of the HPM phase. We examined various crystal structures, including 2M, 10M, 14M, and 4O, as candidates for the HPM phase structure. Righi *et al.* reported that a nonstoichiometric alloy, $Ni_{1.95}Mn_{1.19}Ga_{0.86}$, exhibits a monoclinic-based 10M commensurate structure with a monoclinic angle of $\beta \sim 90.3^\circ$ in the M phase, while a stoichiometric Ni_2MnGa features an orthorhombic-based 10M incommensurate structure in the M phase [34]. Martynov and Kokorin performed x-ray experiments on Ni_2MnGa single crystals under uniaxial compressive and tensile loading, observing monoclinic distortion of 10M- and 14M-like modulations [35]. Kim *et al.* noted that the 10M martensite is known to appear in stoichiometric alloys, while the 14M and 2M martensite appear in nonstoichiometric alloys as the HPM phase in Ni-Mn-Ga systems [22]. Among these structures, the 4O orthorhombic-based, the 10M incommensurate orthorhombic-based, and the 2M tetragonal-based structures could not be indexed as the HMP phase in the present experiment. The remaining two HPM phase candidates are the monoclinic-based 10M and 14M modulated structures with space group of $C2/m$. Therefore, we examined which of the two modulated structures better matched the experimental pattern.

Due to challenges in determining the modulation vector $\boldsymbol{q}$ from the high-pressure x-ray diffraction pattern, we explored the 10M commensurate structure with $\boldsymbol{q} = 2/5\boldsymbol{c}^*$ and the 14M commensurate structure with $\boldsymbol{q} = 3/7\boldsymbol{c}^*$, referencing the findings of Righi *et al.* [34]. Displacive modulations involving the atomic positions of Ni, Mn, and Ga are represented by

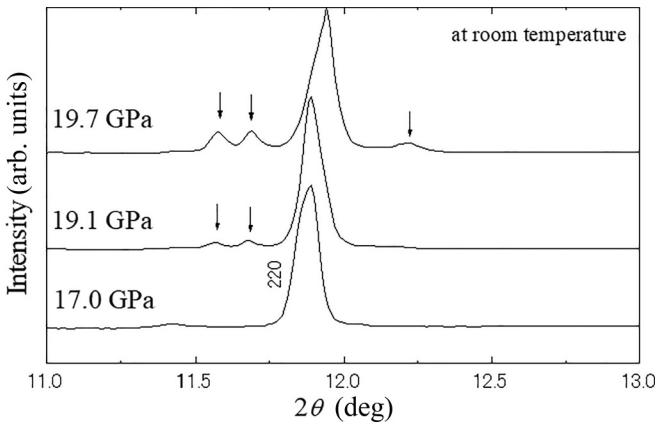

FIG. 3. The RT XRPD patterns of Ni_2MnGa near the 220 main peak at position B under pressure at 17.0, 19.1, and 19.7 GPa.

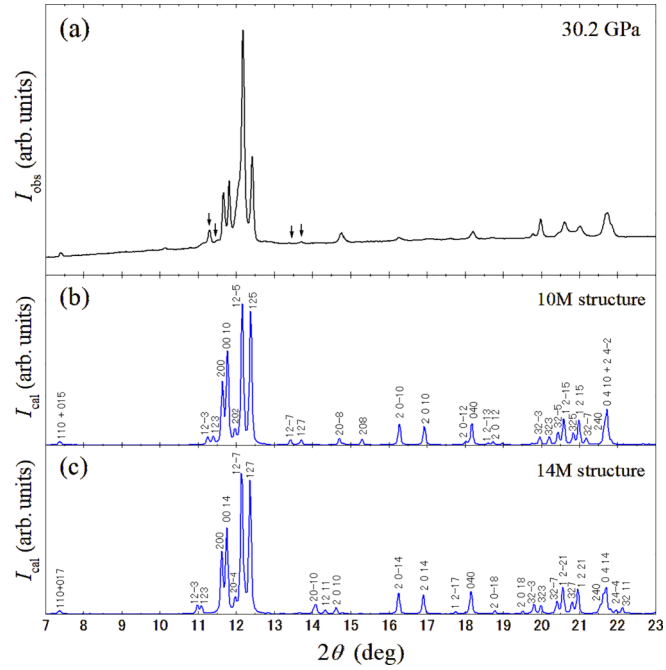

FIG. 4. (a) The experimental x-ray powder diffraction pattern of Ni_2MnGa under a pressure of 30.2 GPa at RT. The down arrows indicate the diffraction line of interest mentioned in the text. (b) The calculated x-ray powder diffraction pattern of Ni_2MnGa with the 10M modulated structure (S.G.: $C2/m$). (c) The calculated x-ray powder diffraction pattern of Ni_2MnGa with the 14M modulated structure (S.G.: $C2/m$).

TABLE I. Atomic coordinates of Ni_2MnGa calculated based on modulated structure for (a) the 10M commensurate structure ($\boldsymbol{q} = 2/5\boldsymbol{c}^*$) and for (b) the 14M commensurate structure ($\boldsymbol{q} = 3/7\boldsymbol{c}^*$). The x coordinates were determined using Eq. (1).

(a)

Atom type	Wyck.	x	y	z
Mn1	2*a*	0.00000	0.00000	0.00000
Mn2	4*i*	0.04115	0.00000	0.20000
Mn3	4*i*	–0.06657	0.00000	0.40000
Ga1	2*b*	0.00000	0.50000	0.00000
Ga2	4*i*	0.04115	0.50000	0.20000
Ga3	4*i*	–0.06657	0.50000	0.40000
Ni1	4*h*	0.50000	0.25000	0.00000
Ni2	8*j*	0.53762	0.25000	0.20000
Ni3	8*j*	0.43913	0.25000	0.40000

(b)

Atom type	Wyck.	x	y	z
Mn1	2*a*	0.00000	0.00000	0.00000
Mn2	4g	0.03037	0.00000	0.28571
Mn3	4g	–0.05473	0.00000	0.39988
Mn4	4g	0.06825	0.00000	0.42857
Ga1	2*b*	0.00000	0.50000	0.00000
Ga2	4g	0.03037	0.50000	0.28571
Ga3	4g	–0.05473	0.50000	0.39988
Ga4	4g	0.06825	0.50000	0.42857
Ni1	4f	0.50000	0.25000	0.00000
Ni2	8h	0.52777	0.25000	0.28571
Ni3	8h	0.44996	0.25000	0.39988
Ni4	8h	0.56240	0.25000	0.42857

sinusoidal waveforms. The atomic positions x_i in the commensurate or incommensurate phase are given by

$$x_i = \bar{x}_i + u_i(\bar{x}_4), \tag{1}$$

$$u_i(\bar{x}_4) = \sum_{n=1}^{\infty} \left\{ A_n^i \sin(2\pi n \bar{x}_4) + B_n^i \cos(2\pi n \bar{x}_4) \right\}, \tag{2}$$

where $\bar{x}_i$ is the general atomic position in the basic structure, u_i defines the modulation function dependent on the $\bar{x}_4$ superspace coordinate for the ith atomic site [34,36], A_n^i and B_n^i are the amplitudes of the displacement modulation, and n is the order of the Fourier series. For simplicity, we set $n = 1$. The x_i values for each atom are obtained by setting $A_1 = 0.07$ for Mn and Ga atoms, $A_1 = 0.064$ for the Ni atom, and $B_1 = 0$ for all atoms, based on previous experiments of 10M and 14M martensite structures at ambient pressure [34,37]. Table I shows the results for each atomic coordinate of 10M and 14M commensurate structures calculated based on Eq. (1). In x-ray diffraction experiments under high pressure using DAC, the peak intensity ratios slightly differ due to statistical inaccuracies in diffraction intensity resulting from a spotty Debye ring or the effect of preferred orientation. Additionally, it has been reported that in the M phase of Ni_2MnGa, close to stoichiometric conditions, various stacking periods other than 10M and 14M might coexist [38], potentially impacting the analysis of the M phase. Consequently, we refrained from employing Rietveld's complete pattern fitting for the experimental results. Instead, profile fitting on each diffraction line was performed to determine the lattice constants of each modulation structure, as presented in Table II.

TABLE II. Crystal data for the martensite structure of Ni_2MnGa at RT under the pressure of 30.2 GPa: (a) for the 10M structure and (b) for the 14M structure.

(a)

Crystal system	Monoclinic (10M)
Space group	$C2/m$
a_m (Å)	4.058(1)
b_m (Å)	5.215(1)
c_m (Å)	20.068(5)
β (deg)	92.239(4)

(b)

Crystal system	Monoclinic (14M)
Space group	$C2/m$
a_m (Å)	4.064 (1)
b_m (Å)	5.220(2)
c_m (Å)	28.129(9)
β (deg)	92.226(6)

In Figs. 4(b) and 4(c), we present the calculated x-ray diffraction patterns for 10M and 14M modulated structures using the program RIETAN-FP [29], comparing them with the experimental pattern in Fig. 4(a). The diffraction intensities and 2θ positions of the main peaks in the two calculated patterns are in good agreement with the experimental pattern. However, some differences in details are observed. First, the two peaks near $2\theta = 11^\circ$ indicated by arrows in Fig. 4(a) can be indexed for 1 2 $\bar{3}$ and 1 2 3 diffractions in the 10M structure in Fig. 4(b), but cannot be indexed in the 14M one in Fig. 4(c). Second, two peaks between $2\theta = 13^\circ$ and 14° can be indexed by 1 2 $\bar{7}$ and 1 2 7 diffractions for the 10M structure, but cannot be indexed for the 14M one. Third, 2 0 $\overline{10}$, 1 2 11, and 2 0 10 diffraction lines near $2\theta = 14^\circ$ seen in the calculated pattern of the 14M structure [Fig. 4(c)] are absent in the experimental pattern of Fig. 4(a). Based on these observations, we conclude that the high-pressure phase of Ni_2MnGa observed in this study is likely to be a 10M modulated structure with an angle of $\beta = 92.2^\circ$, which is larger than the slight monoclinic distortion observed at ambient pressure ($\beta = 90.3^\circ$) [34]. The higher angle of β likely reflects the effect of elastic lattice distortion under high pressure. The 10M modulated structure of stoichiometric Ni_2MnGa alloy under high pressure is consistent with the previous report [22].

The pressure dependencies of lattice parameters for both the LPA phase ($L2_1$ cubic structure) and the HPM phase (10M monoclinic structure) are shown as a function of pressure in Fig. 5. Under increasing pressure, each axial length exhibits a monotonic decrease. Simultaneously, the monoclinic angle β also monotonically increases with pressure. This suggests that under high-pressure conditions, the angle β increases as it undergoes elastic deformation due to external pressure. The measured value of β deviates significantly from the $\beta \sim 90.3^\circ$ observed at atmospheric pressure by Righi

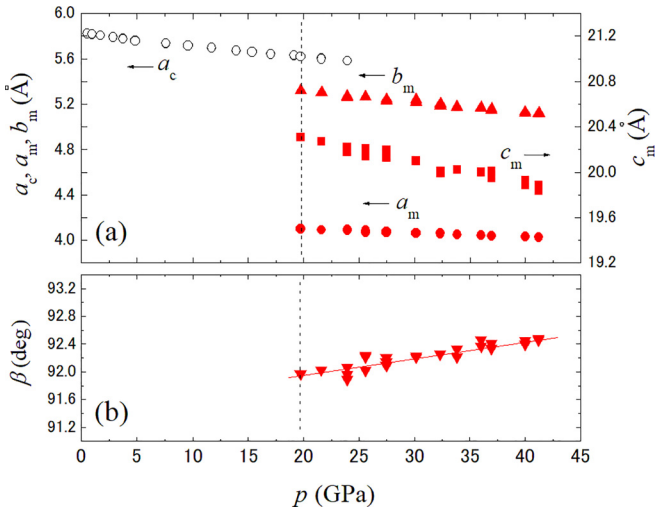

FIG. 5. Pressure dependencies of the lattice parameters for Ni_2MnGa: (a) the axial lengths of a_c in the LPA cubic cell, and of a_m, b_m, c_m in the HPM monoclinic cell; and (b) the angle β between the a_m and c_m axes. The solid red line denotes the result of a least-squares fit. The dashed line denotes the transition pressure. The error bars are covered by the symbols.

et al. [34]. The pressure coefficient of β is determined to be $d\beta/dp = +2.4\times10^{-2}$ deg/GPa by least-squares fitting. Figure 6 shows pressure dependencies of the axial ratios, $c_m/5a_m$ and $b_m/\sqrt{2}\ a_m$, in the HPM monoclinic cell. The pressure coefficients of $c_m/5a_m$ and $b_m/\sqrt{2}\ a_m$ are -1.3×10^{-5} and -1.1×10^{-3}/GPa, respectively. Thus it shows that b_m is more likely to shrink under pressure than c_m. In Fig. 7, the pressure dependences of the interatomic distances d_c(Mn1-Mn1), d_m(Mn1-Mn1), and d_m(Mn2-Mn2) are shown, assuming that the atomic coordinates of the high-pressure phase follow the modulation model of Eqs. (1) and (2). Due to the martensitic transition, d_m(Mn1-Mn1) is elongated from

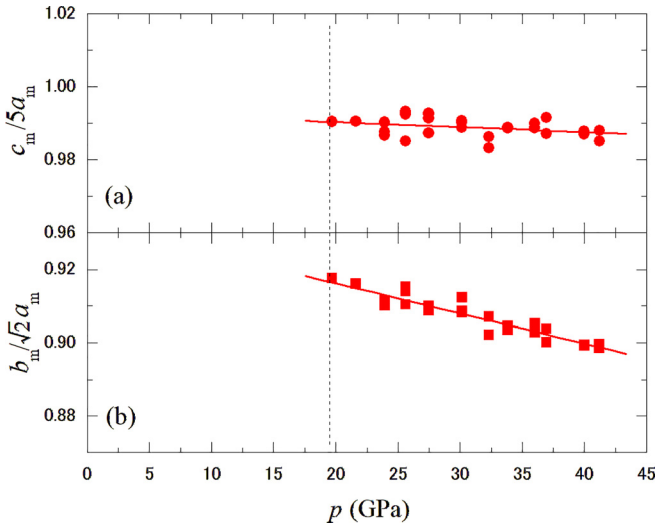

FIG. 6. Pressure dependencies of the axial ratios for Ni_2MnGa: (a) the ratio of $c_m/5a_m$ and (b) the ratio of $b_m/\sqrt{2}a_m$ in the HPM monoclinic cell. The solid red lines denote the results of a least-squares fit. The dashed line denotes the transition pressure. The error bars are covered by the symbols.

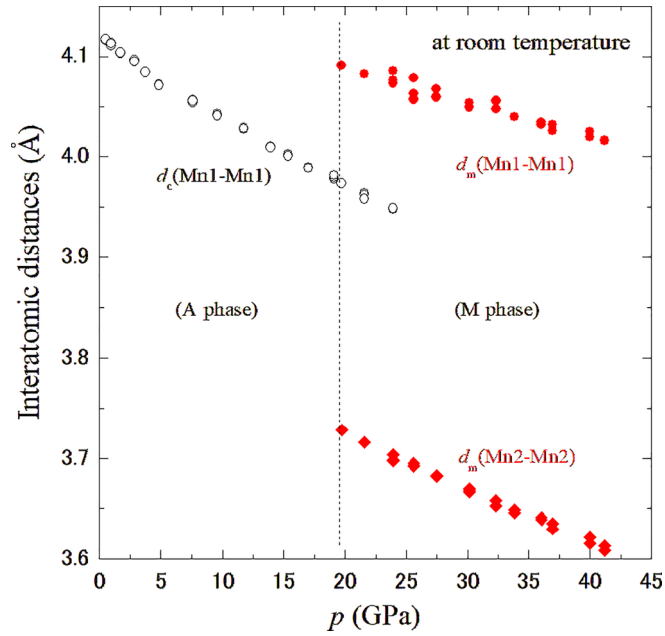

FIG. 7. Pressure dependencies of the interatomic distances d_c(Mn1-M1), d_m(Mn1-M1), and d_m(Mn2-Mn2) for Ni_2MnGa. Here, d_c and d_m denote interatomic distances for the cubic A and monoclinic M phases, respectively. In the A phase, Mn1 denotes the Mn ion at the Wyckoff 4*a* site in the $L2_1$ structure. In the M phase, Mn1 and Mn2 denote the sites listed in Table I. The dashed line denotes the transition pressure. The error bars are covered by the symbols.

d_c(Mn1-Mn1), while the d_m(Mn2-Mn2) becomes the nearest-neighbor Mn-Mn interatomic distance in the HPM phase. All the distances are monotonously shortened with pressure. The effect of this pressure dependence on magnetism will be discussed in the next section.

The pressure dependencies of the volume in the LPA phase and the HPM phase are shown in Fig. 8, indicating a slight volume reduction of $\Delta V/V \sim 0.1\%$ at the transition. This volume reduction is of the same order as estimations of $\Delta V/V = 0.1\%$ observed in a stoichiometric Ni-Mn-Ga alloy using the Clausius-Clapeyron relationship [39], and $\Delta V/V \sim 0.06\%$ observed in a nonstoichiometric Ni-Mn-Ga alloy [40]. The volume change in the martensitic phase transition can be estimated from the Clausius-Clapeyron equation,

$$\frac{dT_M}{dp} = \frac{\Delta V}{\Delta S}. \tag{3}$$

Here ΔV is the difference in molar volume and ΔS is the difference in molar entropy between the HPM and LPA phases at T_M. The value of ΔS at T_M (~200 K) was measured to be -5.2 J/mol K from the latent heat of -4.2 J/g during the structural transition from the austenite cubic structure to the martensite 10M structure [21] for Ni_2MnGa. Using this value and the pressure derivative $dT_M/dp = +8.0$ K/GPa, which will be explained later in the next section, Sec. III B, in Eq. (3), we obtain $\Delta V = -4.1\times10^{-7}$ m^3/mol. The molar volume of the LPA phase at 19.7 GPa is calculated to be $V_A \sim 2.67\times10^{-5}$ m^3/mol from its lattice parameters. Then we obtain $\Delta V/V_A = -0.15\%$, which is mostly the same as $\Delta V/V \sim 0.1\%$ by the high-pressure XRPD experiment. This volume reduction at T_M of Ni_2MnGa is small by nearly a factor of 6

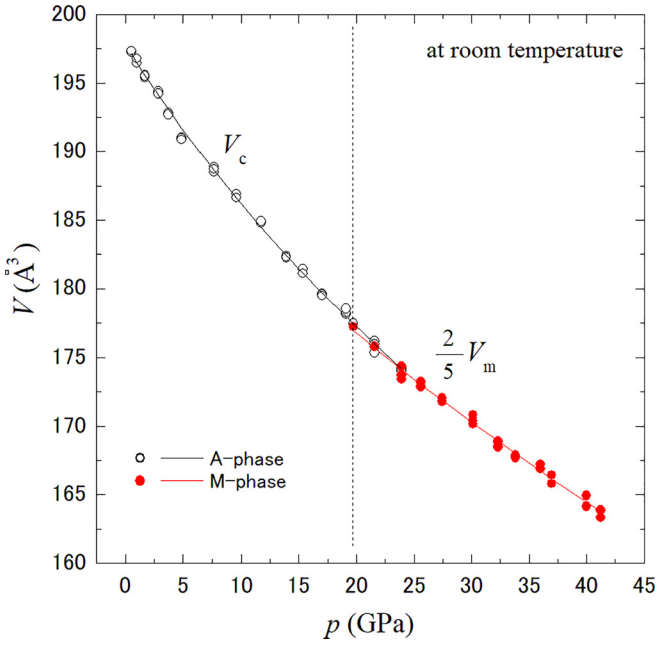

FIG. 8. Pressure dependence of the volume for Ni_2MnGa. Here, V_c is the volume of a cubic cell in the austenite phase and V_m is the volume of a monoclinic cell in the martensite phase. The volume of the high-pressure 10M-monoclinic structure, V_m, is scaled to $2/5V_m$ for comparison with Vc. (The number of formula units in each unit cell, Z, is equal to 4.) Solid lines represent the fitting functions of the Murnaghan EOS applied to the experimental volumes of both phases. The error bars are covered by the symbols.

compared to the value of $\Delta V/V \sim 0.6\%$ for $Ni_2Mn_{1.44}Sn_{0.56}$ [41], where the cubic $L2_1$ structure undergoes a martensitic transition to the orthorhombic 4O structure.

The bulk moduli B_0 and their pressure derivatives B'_0 in both the LPA and the HPM phases were determined by fitting p-V data to the Murnaghan equation of state (EOS) [42],

$$P(V) = \frac{B_0}{B'_0}\left\{\left(\frac{V}{V_0}\right)^{-B'_0} - 1\right\}, \quad (4)$$

where V_0 is the volume at ambient pressure. The obtained values of the B_0 and B'_0 in the LPA phase are 147(2) GPa and 3.8(2), respectively. In Table III, we list a collection of B_0 and B'_0, and elastic constants obtained in the $L2_1$ cubic structure of the austenite phase. All previous experimental values of B_0 were calculated from the elastic constants of c_{11}, c_{12}, and c_{44} measured using ultrasonic measurement (USM). Among them, the B_0 of 146 GPa measured by Worgull *et al.* [44] is almost the same as the B_0 obtained from the present V-P curve. On the other hand, as the theoretical values of B_0 were mostly calculated on the ground state at the temperature of 0 K, they tend to be higher than the values at RT. Considering the temperature dependence according to the literature [49,55,56], the experimental value $B_0 = 147$ can be regarded as almost the same as the calculated ones. Regarding the value of B'_0, calculated values [48,52] show good agreement with the present B'_0 of 3.8(2). On the other hand, the experimental values of B_0, B'_0, and zero pressure volume in the HPM phase were determined to be 229(4) GPa, 1.6(3), and 191(2) Å^3, respectively. In Table IV, we list a collection of B_0 and B'_0 obtained in nonmodulated (NM) and 10M martensitic structures. The B_0 value estimated in this study is about 55% larger than the calculated values based on the modulated 10M and NM tetragonal structures, indicating that the Ni_2MnGa alloy is hardened in the HPM phase. In the future, a more detailed band calculation based on the experimental values of B_0 and B'_0 is desired to understand the cause of the hardening below the PM phase.

TABLE IV. A collection of bulk moduli, and their derivatives obtained in the martensitic structures of NM and 10M for Ni_2MnGa.

Structure	B_0 (GPa)	B'_0	Temperature	Method	Reference
Martensite 10M	229(4)	1.6(3)	RT	This work	–
	153.2	–	0 K	Calc.	[51]
Martensite NM	142.3	–	0 K	USM	[57]
	157.4	–	0 K	Calc.	[49]
	158.0	–	0 K	Calc.	[51]
	155.2	–	0 K	Calc.	[53]

TABLE III. A collection of bulk moduli, their derivatives, and the elastic constants obtained in the $L2_1$ cubic structure for Ni_2MnGa.

B_0 (GPa)	B'_0	c_{11} (GPa)	c_{12} (GPa)	c_{44} (GPa)	Temperature	Method[a]	Reference
147(2)	3.8(2)	–	–	–	RT	This work	–
129	–	213	87	92	300 K	USM	[43]
146	–	152	143	103	300 K	USM	[44]
106.7	–	136	92	102	RT	USM	[9]
147.3	–	156	143	98	225 K	USM	[45]
157.3	–	163.6	155.4	106.7	0 K	Calc.	[46]
161.44	–	165.41	159.45	113.67	0 K	Calc.	[47]
136.88	4.01	–	–	–	0 K	Calc.	[48]
156.7	–	166.7	151.7	113.4	0 K	Calc.	[49]
151.9	–	–	–	99.4	0 K	Calc.	[50]
155.7	–	163	152	107	0 K	Calc.	[51]
206.50	4.13393	214.09	202.7	39.64	0 K	Calc.	[52]
155	–	163	151	110	0 K	Calc.	[53]
155	–	–	–	–	0 K	Calc.	[54]

[a]"USM" and "Calc." denote ultrasonic measurement and first-principles calculation, respectively.

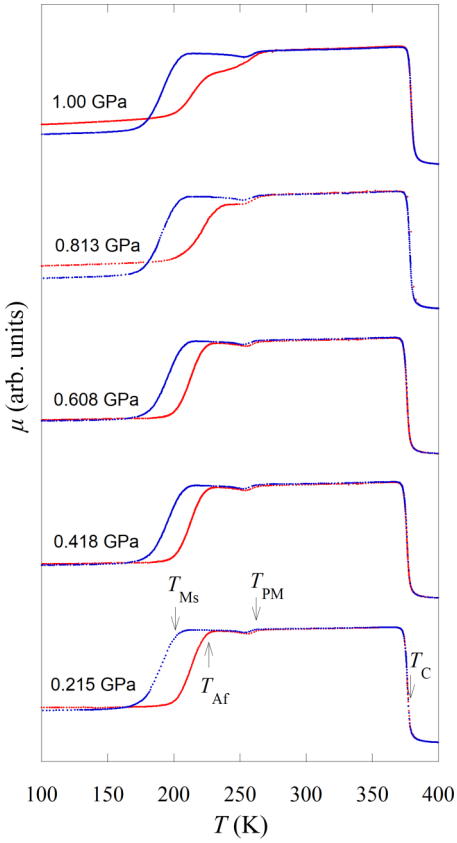

FIG. 9. The initial permeability μ versus temperature curves for Ni_2MnGa at various pressures. The blue and red solid lines denote the data obtained during the cooling and heating processes, respectively.

B. Initial permeability

Figure 9 shows the temperature dependence of the initial permeability μ for Ni_2MnGa under various pressures. The abrupt increase of μ within the temperature range of 350–400 K, as temperature decreases, is attributable to the magnetic phase transition from paramagnetic to ferromagnetic phases. The T_C's were determined as the point where the differential value is maximized on the $\mu(T)$ curve, as depicted in Fig. 9. During the cooling process, around 260 K, noticeable decreases in μ indicate the onset of the PM transition. The transition points (T_{PM}) were defined as the cross points of the linear extrapolation lines from both higher- and lower-temperature ranges on the μ-T curves. Moreover, an abrupt change of $\mu(T)$ around 200 K in Fig. 9 is ascribed to the martensitic transition. The martensitic transition temperature (T_M) was defined using the equation $T_M = (T_{Ms} + T_{Af})/2$, where T_{Ms} and T_{Af} represent the martensitic transition starting temperature and the reverse martensitic transition finishing temperature, respectively. The values of T_{Ms} and T_{Af} were defined as cross points of linear extrapolation lines of the $\mu(T)$ curves from both higher- and lower-temperature ranges. The width of the transition hysteresis is about 20 K, consistent with previous measurements [15,58]. The pressure dependencies of T_C, T_{PM}, and T_M are shown in Fig. 10. All these specific temperatures exhibit a monotonic increase with pressure. The pressure derivatives of these characteristic temperatures,

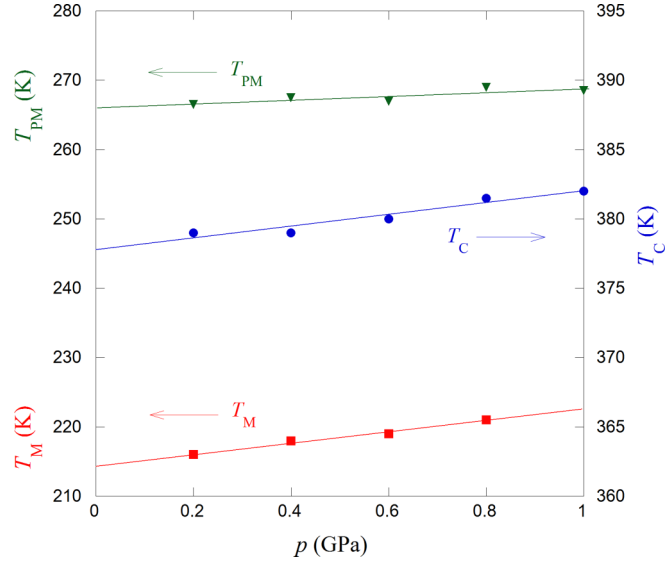

FIG. 10. The pressure dependencies of the Curie temperature T_C, the martensitic transition temperature T_M, and the premartensitic transition temperature T_{PM} for Ni_2MnGa. The solid lines denote the results of least-squares fits for each specific temperature.

denoted as dT_C/dp, dT_{PM}/dp, and dT_M/dp, are estimated to be 4.3, 2.8, and 8.0 K/GPa, respectively. For comparison, Table V includes the characteristic temperatures and their pressure derivatives alongside those from previous experiments.

The dT_C/dp for Ni_2MnGa was estimated to be 4.3 K/GPa at the pressure limit of $p = 0$ GPa in this study. This value is in good accordance with those reported by Kamarád *et al.* [25] and Kanomata *et al.* [59]. The positive value of dT_C/dp for Ni_2MnGa is also consistent with the empirical interaction curves defined by Kanomata *et al.* [24] and Lázpita *et al.* [60], where the magnetic transition temperatures of a series of Heusler alloys increase with decreasing nearest-neighbor Mn-Mn interatomic distance. As seen in Fig. 7, the nearest-neighbor Mn1-Mn1 distance, d_c(Mn1-Mn1), at room temperature for Ni_2MnGa decreases from 4.12 Å at 0.53 GPa to 3.95 Å at 23.9 GPa. Şaşıoğlu *et al.* [61] accounted theoretically for this behavior in terms of the competition between two opposing trends, namely, the stronger effect of increasing carrier hopping compared to the effect of decreasing atomic moments due to the band widening.

As seen in Fig. 10, T_M increases linearly with pressure as a consequence of the lower volume of the M phase with respect to the A phase. The pressure derivative of T_M for Ni_2MnGa is found to be about 8.0 K/GPa, which is almost comparable to that ($dT_M/dp = 6.19$ K/GPa) reported by Devarajan *et al.* [28]. On the other hand, Kamarád *et al.* showed that T_M of Ni_2MnGa is surprisingly stable under pressure ($dT_M/dp < +0.5$ K/GPa) [25]. It should be noted that T_M and its pressure derivative for the Ni-Mn-Ga Heusler alloys are much more sensitive to the composition of alloys. In this study, we observed the martensitic transition of Ni_2MnGa at room temperature by applying the external pressure of 19.1 GPa. Assuming a linear increase in T_M with pressure up to 19.1 GPa, the estimated dT_M/dp is 5.1 K/GPa. This value is consistent with the $dT_M/dp = +8.0$ K/GPa estimated from

TABLE V. A collection of T_C, T_{PM}, and T_M at ambient pressure and their pressure derivatives.

	Composition	T_C (K)	T_{PM} (K)	T_M (K)	dT_C/dp (K/GPa)	dT_{PM}/dp (K/GPa)	dT_M/dp (K/GPa)
This work	Ni_2MnGa	378	266	215	4.3	2.8	8.0
Ref. [20]	Ni_2MnGa	–	–	275	–	–	5.5 ± 0.2
Ref. [21]	$Ni_2Mn_{0.94}Ga_{0.96}$	–	–	∼291	–	–	5.4 ± 0.3
Ref. [25]	Ni_2MnGa	375	–	219	5.9	–	$<+0.5$
Ref. [23]	$Ni_{49.2}Mn_{26.6}Ga_{24.2}$	–	239	180	–	-6 ± 1	–
Ref. [39]	Ni_2MnGa	–	256	201	–	13.1	16.2
Ref. [59]	Ni_2MnGa	∼357	–	–	3.6	–	–
Ref. [28]	Ni_2MnGa	–	–	216	–	–	6.19

the μ versus T curves under pressure (see Fig. 9). It is well known that the Mn-excess $Ni_2Mn_{1.44}Sn_{0.56}$ Heusler alloy also undergoes the martensitic transition at 221 K [62]. In this case, it was observed that T_M increases linearly at the rate of $dT_M/dp = +24$ K/GPa for $Ni_2Mn_{1.44}Sn_{0.56}$ [63]. Such a difference is due to the fact that for Ni_2MnGa the relative volume change at T_M is much smaller than that of $Ni_2Mn_{1.44}Sn_{0.56}$ [7,41]. Regarding the finding of $dT_{PM}/dp \sim 2.8$ K/GPa, on the other hand, it is difficult to compare because the few experimental values show both positive and negative signs. Since the origin of the PM transition is still under discussion, we believe that investigating its pressure dependence will be a focus of future research.

IV. CONCLUSION

We have experimentally investigated the pressure dependencies of phase transitions in the ferromagnetic shape memory alloy Ni_2MnGa by *in situ* angle-dispersive x-ray diffraction using synchrotron radiation and by initial permeability measurement. Our findings reveal that Ni_2MnGa undergoes a structural phase transition from the austenite phase of $L2_1$ structure to the martensite phase of 10M modulated structure with a distortion of $\beta \sim 92^\circ$ at high pressure of approximately 19.1 GPa. The volume reduction at the structural phase transition is nearly 0.1%, which is mostly understood within the framework of the Clausius-Clapeyron relationship. The values of the bulk moduli at room temperature for the low-pressure and high-pressure phases are 147(2) and 229(4) GPa, respectively. In particular, the bulk modulus of the high-pressure martensite phase is ∼55% larger than that of the low-pressure austenite phase. The pressure dependencies of the Curie temperature, the PM transition temperature, and the martensite transition temperature were determined through initial permeability experiments under high pressure, leading to the construction of a pressure-temperature phase diagram. The positive value of dT_C/dp is consistent with established empirical interaction curves, where the magnetic transition temperature of a series of Heusler alloys increases with decreasing nearest-neighbor Mn-Mn interatomic distance. The pressure derivative of T_M in Ni_2MnGa was found to be about 8.0 K/GPa, consistent with previous studies and about one-third of the value observed in the Ni_2MnSn system. Further experiments and first-principles calculations are required to comprehend the large value of bulk modulus under high pressure, as well as the pressure dependencies of characteristic temperatures including the PM transition, from the perspective of electronic, elastic, and magnetic properties.

ACKNOWLEDGMENTS

This work was supported by a research grant from a Grant-in-Aid for Scientific Research of the Japan Society for the Promotion of Science (JSPS, Grants No. 18K04685, No. 19H00648, and No. 22K04677). The synchrotron radiation experiments were performed at SPring-8 with the approval of JASRI (Proposal No. 2021A1079). The authors would like to express their sincere thanks to Ryuji Kouta, Faculty of Engineering, Yamagata University (Yonezawa, Japan), for his help on the sample preparation.

[1] P. J. Webster, K. R. A. Ziebeck, S. L. Town, and M. S. Peak, Magnetic order and phase transformation in Ni_2MnGa, Philos. Mag. B **49**, 295 (1984).

[2] K. Ullakko, J. K. Huang, C. Kantner, R. C. O'Handley, and V. V. Kokorin, Large magnetic-field-induced strains in Ni_2MnGa single crystals, Appl. Phys. Lett. **69**, 1966 (1996).

[3] O. Tegus, E. Brück, L. Zhang, W. Dagula, K. H. J. Buschow, and F. R. de Boer, Magnetic-phase transitions and magnetocaloric effects, Physica B (Amsterdam) **319**, 174 (2002).

[4] V. V. Khovaylo, K. P. Skokov, Yu. S. Koshkid'ko, V. V. Koledov, V. G. Shavrov, V. D. Buchelnikov, S. V. Taskaev, H. Miki, T. Takagi, and A. N. Vasiliev, Adiabatic temperature change at first-order magnetic phase transitions: $Ni_{2.19}Mn_{0.81}Ga$ as a case study, Phys. Rev. B **78**, 060403(R) (2008).

[5] P. J. Brown, J. Crangle, T. Kanomata, M. Matsumoto, K.-U. Neumann, B. Ouladdiaf, and K. R. A. Ziebeck, The crystal structure and phase transitions of the magnetic shape memory compound Ni_2MnGa, J. Phys.: Condens. Matter **14**, 10159 (2002).

[6] S. Singh, J. Nayak, A. Rai, P. Rajput, A. H. Hill, S. R. Barman, and D. Pandey, (3 + 1)D superspace description of the incommensurate modulation in the premartensite phase of Ni_2MnGa: A high resolution synchrotron x-ray powder diffraction study, J. Phys.: Condens. Matter **25**, 212203 (2013).

[7] S. Singh, J. Bednarcik, S. R. Barman, C. Felser, and D. Pandey, Premartensite to martensite transition and its implications for the origin of modulation in Ni_2MnGa ferromagnetic shape-memory alloy, Phys. Rev. B **92**, 054112 (2015).

[8] V. V. Kokorin, V. A. Chernenko, E. Cesari, J. Pons, and C. Segui, Pre-martensitic state in Ni-Mn-Ga alloys, J. Phys.: Condens. Matter **8**, 6457 (1996).

[9] L. Manosa, A. Gonzalez-Comas, E. Obrado, A. Planes, V. A. Chernenko, V. V. Kokorin, and E. Cesari, Anomalies related to the TA_2-phonon-mode condensation in the Heusler Ni_2MnGa alloy, Phys. Rev. B **55**, 11068 (1997).

[10] H. Seiner, V. Kopecký, M. Landa, and O. Heczko, Elasticity and magnetism of Ni_2MnGa premartensitic tweed, Phys. Status Solidi B **251**, 2097 (2014).

[11] A. Zheludev, S. M. Shapiro, P. Wochner, A. Schwartz, M. Wall, and L. E. Tanner, Phonon anomaly, central peak, and microstructures in Ni_2MnGa, Phys. Rev. B **51**, 11310 (1995).

[12] U. Stuhr, P. Vorderwisch, V. V. Kokorin, and P-A. Lindgard, Premartensitic phenomena in the ferro- and paramagnetic phases of Ni_2MnGa, Phys. Rev. B **56**, 14360 (1997).

[13] V. V. Khovaylo, K. Oikawa, C. Wedel, T. Takagi, T. Abe, and K. Sugiyama, Influence of intermartensitic transitions on transport properties of $Ni_{2.16}Mn_{0.84}Ga$ alloy, J. Phys.: Condens. Matter **16**, 1951 (2004).

[14] A. Cakir, L. Righi, F. Albertini, M. Acet, M. Farle, and S. Aktürk, Extended investigation of intermartensitic transitions in Ni-Mn-Ga magnetic shape memory alloys: A detailed phase diagram determination, J. Appl. Phys. **114**, 183912 (2013).

[15] T. Eto, X. Xu, T. Ito, F. Honda, D. X. Li, G. Oomi, F. Nakamura, H. Masumoto, R. Kainuma, and T. Kanomata, Martensitic and magnetic transitions in $Ni_{2+x}MnGa_{1-x}$ ferromagnetic shape memory alloys, J. Alloys Compd. **871**, 159480 (2021).

[16] A. N. Vasil'ev, A. D. Bozhko, V. V. Khovailo, I. E. Dikshtein, V. G. Shavrov, V. D. Buchelnikov, M. Matsumoto, S. Suzuki, T. Takagi, and J. Tani, Structural and magnetic phase transitions in shape-memory alloys $Ni_{2+x}Mn_{1-x}Ga$, Phys. Rev. B **59**, 1113 (1999).

[17] V. V. Khovaylo, V. D. Buchelnikov, R. Kainuma, V. V. Koledov, M. Ohtsuka, V. G. Shavrov, T. Takagi, S. V. Taskaev, and A. N. Vasiliev, Phase transitions in $Ni_{2+x}Mn_{1-x}Ga$ with a high Ni excess, Phys. Rev. B **72**, 224408 (2005).

[18] V. D. Buchelnikov, V. V. Sokolovskiy, H. C. Herper, H. Ebert, M. E. Gruner, S. V. Taskaev, V. V. Khovaylo, A. Hucht, A. Dannenberg, M. Ogura, H. Akai, M. Acet, and P. Entel, First-principles and Monte Carlo study of magnetostructural transition and magnetocaloric properties of $Ni_{2+x}Mn_{1-x}Ga$, Phys. Rev. B **81**, 094411 (2010).

[19] B. Dutta, A. Cakir, C. Giacobbe, A. Al-Zubi, T. Hickel, M. Acet, and J. Neugebauer, *Ab initio* prediction of martensitic and intermartensitic phase boundaries in Ni-Mn-Ga, Phys. Rev. Lett. **116**, 025503 (2016).

[20] V. A. Chernenko and V. A. L'vov, Thermodynamics of martensitic transformations affected by hydrostatic pressure, Philos. Mag. A **73**, 999 (1996).

[21] V. A. Chernenko, V. V. Kokorin, O. M. Babii, and I. K. Zasimchuk, Phase diagrams in the Ni-Mn-Ga system under compression, Intermetallics **6**, 29 (1998).

[22] J.-H. Kim, T. Taniguchi, T. Fukuda, and T. Kakeshita, Effect of hydrostatic pressure on P-14M-2M and P-2M martensitic transformations in single crystalline Ni-Mn-Ga ferromagnetic shape memory alloys, Mater. Trans. **46**, 1928 (2005).

[23] V. A. Chernenko, S. Besseghini, T. Kanomata, H. Yoshida, and T. Kakeshita, Effect of high hydrostatic pressure on premartensitic transition in Ni_2MnGa, Scr. Mater. **55**, 303 (2006).

[24] T. Kanomata, K. Shirakawa, and T. Kaneko, Effect of hydrostatic pressure on the Curie temperature of the Heusler alloys Ni_2MnZ (Z = Al, Ga, In, Sn and Sb), J. Magn. Magn. Mater. **65**, 76 (1987).

[25] J. Kamarád, F. Albertini, Z. Arnold, F. Casoli, L. Pareti, and A. Paoluzi, Effect of hydrostatic pressure on magnetization of $Ni_{2+x}Mn_{1-x}Ga$ alloys, J. Magn. Magn. Mater. **290–291**, 669 (2005).

[26] F. Albertini, J. Kamarád, Z. Arnold, L. Pareti, E. Villa, and L. Righi, Pressure effects on the magnetocaloric properties of Ni-rich and Mn-rich Ni_2MnGa alloys, J. Magn. Magn. Mater. **316**, 364 (2007).

[27] K. Mandal, D. Pal, N. Scheerbaum, J. Lyubina, and O. Gutfleisch, Effect on pressure on the magnetocaloric properties of nickel-rich Ni-Mn-Ga Heusler alloys, J. Appl. Phys. **105**, 073509 (2009).

[28] U. Devarajan, S. E. Muthu, S. Arumugam, S. Singh, and S. R. Barman, Investigation of the influence of hydrostatic pressure on the magnetic and magnetocaloric properties of $Ni_{2-x}Mn_{1+x}Ga$ (X = 0, 0.15) Heusler alloys, J. Appl. Phys. **114**, 053906 (2013).

[29] F. Izumi and K. Momma, Three-dimensional visualization in powder diffraction, Solid State Phenom. **130**, 15 (2007).

[30] N. Hirao, S. I. Kawaguchi, K. Hirose, K. Shimizu, E. Ohtani, and Y. Ohishi, New developments in high-pressure x-ray diffraction beamline for diamond anvil cell at SPring-8, Matter Radiat. Extremes **5**, 018403 (2020).

[31] C. S. Zha, H. Mao, and R. J. Hemley, Elasticity of MgO and a primary pressure scale to 55 GPa, Proc. Natl. Acad. Sci. USA **97**, 13494 (2000).

[32] Y. Adachi, T. Watanabe, T. Kanomata, M. Hayasaka, K. Endo, H. Nishihara, X. Xu, and R. Kainuma, Effect of pressure on the Curie temperature of Mn_2RuSn and Mn_2PdSn, Physica B (Amsterdam) **511**, 99 (2017).

[33] K. Takemura and A. Dewaele, Isothermal equation of state for gold with a He-pressure medium, Phys. Rev. B **78**, 104119 (2008).

[34] L. Righi, F. Albertini, L. Pareti, A. Paoluzi, and G. Calestani, Commensurate and incommensurate "5M" modulated crystal structures in Ni–Mn–Ga martensitic phases, Acta Mater. **55**, 5237 (2007).

[35] V. V. Martynov and V. V. Kokorin, The crystal structure of thermally- and stress-induced martensites in Ni_2MnGa single crystals, J. Phys. III **2**, 739 (1992).

[36] A. T. Zayak and P. Entel, Role of shuffles and atomic disorder in Ni–Mn–Ga, Mater. Sci. Eng.: A **378**, 419 (2004).

[37] S. Singh, V. Petricek, P. Rajput, A. H. Hill, E. Suard, S. R. Barman, and D. Pandey, High-resolution synchrotron x-ray powder diffraction study of the incommensurate modulation in the martensite phase of Ni_2MnGa: Evidence for nearly 7M modulation and phason broadening, Phys. Rev. B **90**, 014109 (2014).

[38] J. Pons, R. Santamarta, V. A. Chernenko, and E. Cesari, HREM study of different martensitic phases in Ni–Mn–Ga alloys, Mater. Chem. Phys. **81**, 457 (2003).

[39] H. Maeda, T. Fukuda, and T. Kakeshita, Effect of hydrostatic pressure on martensitic transformation in a ferromagnetic shape memory alloy Ni_2MnGa, J. Alloys Compd. **509**, 7840 (2011).

[40] R. Ranjan, S. Banik, S. R. Barman, U. Kumar, P. K. Mukhopadhyay, and D. Pandey, Powder x-ray diffraction study of the thermoelastic martensitic transition in $Ni_2Mn_{1.05}Ga_{0.95}$, Phys. Rev. B **74**, 224443 (2006).

[41] T. Kanomata, K. Fukushima, H. Nishihara, R. Kainuma, W. Itoh, K. Oikawa, K. Ishida, K.-U. Neumann, and K. R. A. Ziebeck, Magnetic and crystallographic properties of shape memory alloys $Ni_2Mn_{1+x}Sn_{1-x}$, Mater. Sci. Forum **583**, 119 (2008).

[42] F. D. Murnaghan, The compressibility of media under extreme pressures, Proc. Natl. Acad. Sci. USA **30**, 244 (1944).

[43] A. N. Vasil'ev, V. V. Kokorin, Y. I. Savchenko, and V. A. Chernenko, The magnetoelastic properties of a Ni_2MnGa single crystal, Zh. Eksp. Teor. Fiz. **98**, 1437 (1990) [Sov. Phys. JETP **71**, 803 (1990)].

[44] J. Worgull, E. Petti, and J. Trivisonno, Behavior of the elastic properties near an intermediate phase transition in Ni_2MnGa, Phys. Rev. B **54**, 15695 (1996).

[45] T. E. Stenger and J. Trivisonno, Ultrasonic study of the two-step martensitic phase transformation in Ni_2MnGa, Phys. Rev. B **57**, 2735 (1998).

[46] H-L. Yan, Y. Zhao, H-X. Liu, M-J. Zhang, H-F. Zhang, J. Bai, N. Jia, B. Yang, Z-B. Li, Y-D. Zhang, C. Esling, X. Zhao, and L. Zuo, *Ab-initio* revelation on the origins of Ti substitution for Ga, Mn and Ni on ferromagnetism, phase stability and elastic properties in Ni_2MnGa, J. Alloys Compd. **821**, 153481 (2020).

[47] T. Roy, D. Pandey, and A. Chakrabarti, Probing the possibility of coexistence of martensite transition and half-metallicity in Ni and Co-based full-Heusler alloys: An *ab initio* calculation, Phys. Rev. B **93**, 184102 (2016).

[48] Y. Qawasmeh and B. Hamad, Investigation of the structural, electronic, and magnetic properties of Ni-based Heusler alloys from first principles, J. Appl. Phys. **111**, 033905 (2012).

[49] C-M. Li, H-B. Luo, Q-M. Hu, R. Yang, B. Johansson, and L. Vitos, Temperature dependence of elastic properties of $Ni_{2+x}Mn_{1-x}Ga$ and $Ni_2Mn(Ga_{1-x}Al_x)$ from first principles, Phys. Rev. B **84**, 174117 (2011).

[50] Q-M. Hu, C-M. Li, S. E. Kulkova, R. Yang, B. Johansson, and L. Vitos, Magnetoelastic effects in $Ni_2Mn_{1+x}Ga_{1-x}$ alloys from first-principles calculations, Phys. Rev. B **81**, 064108 (2010).

[51] S. O. Kart and T. Cagın, Elastic properties of Ni_2MnGa from first-principles calculations, J. Alloys Compd. **508**, 177 (2010).

[52] H. Rached, D. Rached, R. Khenata, A. H. Reshak, and M. Rabah, First-principles calculations of structural, elastic and electronic properties of Ni_2MnZ (Z = Al, Ga and In) Heusler alloys, Phys. Status Solidi B **246**, 1580 (2009).

[53] S. Özdemir Kart, M. Uludoğan, I. Karaman, and T. Çağın, DFT studies on structure, mechanics and phase behavior of magnetic shape memory alloys: Ni_2MnGa, Phys. Status Solidi A **205**, 1026 (2008).

[54] C. Bungaro, K. M. Rabe, and A. DalCorso, First-principles study of lattice instabilities in ferromagnetic Ni_2MnGa, Phys. Rev. B **68**, 134104 (2003).

[55] G-L. Xu, J-D. Chen, D. Chen, J-Z. Ma, B-H. Yu, and D-H. Shi, First-principles calculation of elastic and thermodynamic properties of Ni_2MnGa Heusler alloy, Chin. Phys. B **18**, 744 (2009).

[56] W. Peng, D. H. Zhang, and N. Xu, Bulk modulus and thermodynamic properties of $L2_1$ Ni_2XY (X = Mn, Fe, Co, Y=Ga, In) compounds studied by first-principles calculations, J. Mater. Sci. **52**, 1149 (2017).

[57] P. Sedlák, H. Seiner, L. Bodnárová, O. Heczko, and M. Landa, Elastic constants of non-modulated Ni-Mn-Ga martensite, Scr. Mater. **136**, 20 (2017).

[58] X. Xu, M. Nagasako, W. Ito, R. Y. Umetsu, T. Kanomata, and R. Kainuma, Magnetic properties and phase diagram of $Ni_{50}Mn_{50-x}Ga_x$ ferromagnetic shape memory alloys, Acta Mater. **61**, 6712 (2013).

[59] T. Kanomata, S. Kyuji, O. Nashima, F. Ono, T. Kaneko, and S. Endo, The Curie temperature in Heusler alloys Ni_2MnZ (Z = Ga, Sn and Sb) under high pressure, J. Alloys Compd. **518**, 19 (2012).

[60] P. Lázpita, V. A. L'vov, J. Rodríguez Fernáandez, J. M. Barandiaráan, and V. A. Chernenko, Combined effect of magnetic field and hydrostatic pressure on the phase transitions exhibited by Ni-Mn-In metamagnetic shape memory alloy, Acta Mater. **193**, 1 (2020).

[61] E. Şaşıoğlu, L. M. Sandratskii, and P. Bruno, Pressure dependence of the Curie temperature in Ni_2MnSn Heusler alloy: A first-principles study, Phys. Rev. B **71**, 214412 (2005).

[62] P. J. Brown, A. P. Gandy, K. Ishida, R. Kainuma, T. Kanomata, K.-U. Neumann, K. Oikawa, B. Ouladdiaf, and K. R. A. Ziebeck, The magnetic and structural properties of the magnetic shape memory compound $Ni_2Mn_{1.44}Sn_{0.56}$, J. Phys.: Condens. Matter **18**, 2249 (2002).

[63] F. T. Yasuda, T. Kanomata, T. Saito, H. Yosida, H. Nishihara, R. Kainuma, K. Oikawa, K. Ishida, K.-U. Neumann, and K. R. A. Ziebeck, Pressure effect on transformation temperatures of ferromagnetic shape memory alloy $Ni_{50}Mn_{36}Sn_{14}$, J. Magn. Magn. Mater. **310**, 2770 (2007).